



Spatiotemporal pattern evolution on a spatial fractional Rosenzweig-MacArthur model

Yong Ye¹ · Jiaying Zhou^{1,2}

Received: 4 December 2024 / Revised: 15 April 2025 / Accepted: 6 June 2025 /

Published online: 20 June 2025

© Università degli Studi di Napoli "Federico II" 2025

Abstract

The Rosenzweig-MacArthur model, which only considers classical diffusion, has long been pointed out as not having the conditions to generate Turing patterns. However, spatial patterns are not limited to one type of Turing pattern. Under appropriate parameters and initial conditions, the model can still observe other spatiotemporal patterns, such as concentric wave patterns, spiral patterns, and lattice formations. This paper extends the model that originally only considered integer diffusion to the case of fractional diffusion. Theoretically, we have analyzed the existence and stability of the equilibria within the model. Furthermore, we have engaged in comprehensive discussions regarding potential transcritical bifurcation, Hopf bifurcation, and stable limit cycle in the absence of diffusion. Notably, the Hopf bifurcation observed in the spatial fractional model lays the groundwork for our subsequent identification of spatiotemporal patterns. Our analysis reveals that fractional diffusion does not change the conclusion that the model does not produce Turing patterns. Still, it plays an important role in the evolution of spatiotemporal patterns. Specifically, in two-dimensional (2D) space, fractional order controls switch between spiral patterns and concentric waves. In addition, lattice formations have been captured within this spatial fractional model, with the fractional order and initial values impacting the spatial distribution of the population. Unlike previously observed, as the predator's diffusion rate increases, despite the parameter values meeting the conditions for model instability, the population density within the region transitions from its original periodic oscillation to a stable state. Intriguingly, spiral patterns persist in three-dimensional (3D) space, where fractional orders govern the formation of 3D lattices. These findings contribute to the enrichment of existing research.

✉ Jiaying Zhou
zhoujy@njfu.edu.cn

Yong Ye
13339239813@163.com

¹ Independent Researcher, Nanjing 210037, Jiangsu, China

² College of Science, Nanjing Forestry University, Nanjing 210037, Jiangsu, China

Keywords Rosenzweig-MacArthur model · Fractional diffusion · Concentric wave · Spiral patterns · Lattice formations · 3D patterns

Mathematics Subject Classification 92D25

1 Introduction

The interaction between predator and prey species is critical to maintaining ecosystem sustainability. Therefore, the population dynamics of predator-prey models have been extensively studied since the seminal work of Lotka and Volterra [1]. Researchers have delved into two primary areas. On the one hand, they continuously introduced new functional response functions, increasing the predator-prey model's dynamic complexity. For example, in 2001, Xiao and Ruan conducted a global analysis of the predator-prey model with a nonmonotonic functional response function. By selecting appropriate control parameters, it was found that the model exhibits various bifurcation phenomena, including saddle-node bifurcation, supercritical and subcritical Hopf bifurcation, and homoclinic bifurcation [2]. In the same year, they also conducted dynamic analysis on the origin of a predator-prey model with a ratio-dependent functional response. They proved that the origin is indeed a high-order critical point. Various topological structures can be near the origin, including parabolic orbits, elliptical orbits, hyperbolic orbits, and any combination of them [3]. This type of work has always been of interest to researchers, especially in recent years, Xiang and his colleagues have conducted a more in-depth analysis of the Holling-Tanner model considering harvesting term and the Holling-Tanner model with generalist predator and prey refuge, respectively. They provided possibilities for the existence of codimension 4 Bogdanov-Takens bifurcation and three types of homoclinic orbits (homoclinic to hyperbolic saddle, saddle-node or neutral saddle) in interacting population systems [4, 5]. Most of these studies are based on mathematical theories to analyze the temporal dynamic behavior of models (stability, boundedness, bifurcation, limit cycles) and other related scientific issues [6].

On the other hand, given the differences in species distribution, it is obvious that there are differences in the distribution of biological populations in different regions [7–9]. At this point, the modeling of reaction-diffusion equations can reflect the spatial distribution of populations and inter-regional flows. Therefore, the study of pattern formation on reaction-diffusion model emerged and has been continuously explored by researchers. The discovery of spatiotemporal patterns can be traced back to 1952. Turing found that the difference in diffusion constants of activators and inhibitors can lead to changes in spatial uniform steady states, and further observed the emergence of periodic spatial patterns [10]. Since then, the study of spatial pattern formation in population and infectious disease models has been widely developed. Specifically, in 2013, Yuan et al. analyzed the pattern formation on a predator-prey model with prey groups. They found that when the mortality rate of predators is used as a control parameter, different mortality rates lead to varying levels of pattern evolution [11]. As a common phenomenon in social environments, time delay has also been studied and added to model research. Surprisingly, in 2009, Sen et al. reported that

small delays may lead to Turing instability in the model studied, resulting in the formation of complex spatial patterns [12]. In 2014, Zhang and his collaborators pointed out in their work the possibility of spatial patterns arising from large delays [13]. Subsequently, there has been sufficient development in the study of pattern formation on reaction-diffusion systems with delays [14–16]. However, most existing research has focused on Turing patterns in spatial reaction-diffusion systems. Many existing models themselves do not have the conditions to generate Turing instability. For instance, the two biological mechanisms envisioned in the Rosenzweig-MacArthur model, namely the logical growth of prey and the saturation functional response of predators, did not contribute to the emergence of diffusion instability. In other words, if the model only considers classical diffusion, it will not generate Turing patterns [17]. Significantly, spatial patterns are not limited to Turing patterns, and Turing instability is not the only condition for generating spatial patterns. For this consideration, in 2012, Nagano and Maeda discovered a series of beautiful patterns, such as spiral patterns, concentric waves, and lattice formations, by selecting appropriate parameters in a model that does not have Turing instability conditions, namely Rosenzweig-MacArthur model. They also emphasized the importance of initial conditions in the formation of these patterns [18].

Our focus lies on the research findings of Sims et al. in 2008, which revealed that animal movement on extensive spatial scales or extended time scales can lead to the establishment of a novel random walking model called the Lévy flight. This model suggests that animals exhibit abnormal diffusion during their movements [19]. Inspired by this finding, numerous studies on fractional-order reaction-diffusion systems have emerged in recent years [20–23]. More specifically, Liu et al. studied a predator-prey model with super-diffusion. The amplitude equation at the Turing-Hopf bifurcation point was obtained using weak nonlinear analysis methods. In addition, by analyzing the amplitude equation under appropriate conditions, rich spatiotemporal dynamics are provided [24–26]. Around 2022, Bi and his co-authors theoretically derived amplitude equations for two-dimensional (2D) and three-dimensional (3D) Turing patterns using the predator-prey model as their research background and discussed the selection and stability of different modes. Numerically, they discovered numerous beautiful patterns, especially the tubes, lamellae, and spherical droplets in 3D patterns, as well as their deformation and mixing structures [27–29]. Similar to the study of spatial integer reaction-diffusion models, we also found little attention to studying spatiotemporal patterns that do not possess Turing instability systems. So, we still take Rosenzweig-MacArthur model as the research background and focus on the following issues: What role does the initial value play in spatiotemporal patterns? Can fractional diffusion still capture specific spatiotemporal patterns such as spirals, concentric waves, and lattice patterns? What is the impact of fractional order on spatiotemporal patterns? Can specific spatiotemporal patterns still be captured in 3D space? This work explores the potential factors affecting the spatiotemporal patterns of non-Turing categories in fractional reaction-diffusion models.

The remaining part of this paper is organized as follows. In Section 2, we present the description and definition of the model. In Section 3, we analyze the stability of the equilibria in the non-diffusion model and the bifurcations around these equilibria. In Section 4, we prove the existence of Hopf bifurcation in the fractional spatial model

Table 1 Biological significance of variables or parameters in model (1)

Variable or parameter	Description
\bar{u}	The density of prey species
\bar{v}	The density of predator species
t	Time
d_u	The diffusion coefficient of prey species
d_v	The diffusion coefficient of predator species
a	The intrinsic growth rate of prey species
K	The carrying capacity of prey species
b	The maximum uptake rate
c	The half-saturation prey density
m	The predator species birth rate
n	The predator species death rate

and capture various complex spatiotemporal patterns through numerical experiments. Finally, a brief discussion is presented in Section 5.

2 Model description and definition

To study the spatiotemporal pattern in the spatial fractional predator-prey model, we adopted the well-known model of Rosenzweig and MacArthur [30] and taking into account fractional diffusion, the following form is obtained:

$$\begin{cases} \frac{\partial \bar{u}}{\partial t} = a\bar{u} \left(1 - \frac{\bar{u}}{K}\right) - \frac{b\bar{u}\bar{v}}{c+\bar{u}} + d_{\bar{u}} \nabla^q \bar{u}, & (x, y) \in \Omega, \quad t > 0, \\ \frac{\partial \bar{v}}{\partial t} = \frac{m\bar{u}\bar{v}}{c+\bar{u}} - n\bar{v} + d_{\bar{v}} \nabla^q \bar{v}, & (x, y) \in \Omega, \quad t > 0, \\ \frac{\partial \bar{u}}{\partial \eta} = \frac{\partial \bar{v}}{\partial \eta} = 0, & (x, y) \in \partial\Omega, \quad t > 0, \\ \bar{u}(x, y, 0) = \bar{u}_0 > 0, \quad \bar{v}(x, y, 0) = \bar{v}_0 > 0, & (x, y) \in \Omega, \end{cases} \quad (1)$$

where Ω is a bounded domain in \mathbb{R}^n with a smooth boundary $\partial\Omega$ and η is the outward unit normal vector along $\partial\Omega$. When $n = 2$, the bounded domain is two-dimensional and can be represented as $(x, y) \in \Omega$ like in model (1). If $n = 3$, the bounded domain is three-dimensional and can be represented as $(x, y, z) \in \Omega$ like in [29]. The boundary condition under consideration is a homogeneous Neumann boundary condition, which means there is no flux on the boundary. To intuitively reflect the biological significance of each variable and parameter, we have summarized it in Table 1.

Some remarks on model (1) are presented below:

- For $q \in (1, 2)$, the fractional derivative describes super-diffusion processes, where individuals exhibit Lévy flight-like movement patterns. In the context of population dynamics, super-diffusion (rather than classical diffusion) has been employed as a more appropriate way to describe the motion of animals under certain circumstances. Classical diffusion models are insufficient for capturing the long-distance

migration processes of populations, which has led to the proposal of super-diffusion models (spatial fractional models) [22, 29].

- The assumption of identical fractional orders q for both predator and prey populations is motivated by two key considerations. First, empirical observations in many ecosystems reveal that predator and prey movements are often governed by analogous environmental constraints, such as habitat fragmentation and resource distribution patterns. For instance, both species may exhibit correlated super-diffusion dispersal behaviors due to shared landscape heterogeneity [27–29]. Second, from a theoretical standpoint, assigning distinct orders would introduce asymmetric coupling into the reaction-diffusion framework, thereby complicating analyses of spatiotemporal pattern formation and system stability. This simplification serves as a foundational step to investigate the role of fractional dynamics in predator-prey interactions.

For the convenience of subsequent theoretical analysis, we have made model (1) dimensionless to achieve the goal of reducing parameters. The transformation form of all variables and parameters is: $\bar{u} = KU$, $\bar{v} = \frac{acV}{b}$, $\frac{K}{c} = \beta$, $A = \frac{a}{m}$, $\gamma = \frac{n}{m}$, $mt = T$, $d_{\bar{u}} = D_U$, $d_{\bar{v}} = D_V$, and $q = \alpha$.

$$\begin{cases} \frac{\partial U}{\partial T} = AU \left[(1 - U) - \frac{V}{1 + \beta U} \right] + D_U \nabla^\alpha U, & (x, y) \in \Omega, \quad T > 0, \\ \frac{\partial V}{\partial T} = V \left(\frac{\beta U}{1 + \beta U} - \gamma \right) + D_V \nabla^\alpha V, & (x, y) \in \Omega, \quad T > 0, \\ \frac{\partial U}{\partial \eta} = \frac{\partial V}{\partial \eta} = 0, & (x, y) \in \partial \Omega, \quad T > 0, \\ U(x, y, 0) = V_0 > 0, \quad V(x, y, 0) = V_0 > 0, & (x, y) \in \Omega, \end{cases} \quad (2)$$

where ∇^α ($1 < \alpha < 2$, $(x, y) \in \mathbb{R}^2$) is the fractional operator and the anomalous diffusion operator ∇^α could be given by the Riesz fractional derivative as

$$\begin{aligned} \nabla^\alpha U &= \frac{\partial^\alpha U}{\partial |x|^\alpha} + \frac{\partial^\alpha U}{\partial |y|^\alpha} \\ &= -\frac{1}{2 \cos(\pi\alpha/2)} \left({}_{RL}D_{-\infty,x}^\alpha U + {}_{RL}D_{x,+\infty}^\alpha U \right) \\ &\quad - \frac{1}{2 \cos(\pi\alpha/2)} \left({}_{RL}D_{-\infty,y}^\alpha U + {}_{RL}D_{y,+\infty}^\alpha U \right). \end{aligned}$$

Considering that the definitions of ${}_{RL}D_{-\infty,x}^\alpha U$, ${}_{RL}D_{x,+\infty}^\alpha U$ and ${}_{RL}D_{-\infty,y}^\alpha U$, ${}_{RL}D_{y,+\infty}^\alpha U$ are similar, we define ${}_{RL}D_{-\infty,x}^\alpha U$ and ${}_{RL}D_{x,+\infty}^\alpha U$ as follows:

$$\begin{aligned} {}_{RL}D_{-\infty,x}^\alpha U &= \frac{1}{\Gamma(2 - \alpha)} \frac{\partial^2}{\partial x^2} \int_{-\infty}^x (x - s)^{1-\alpha} U(s, y, t) ds, \\ {}_{RL}D_{x,+\infty}^\alpha U &= \frac{1}{\Gamma(2 - \alpha)} \frac{\partial^2}{\partial x^2} \int_x^{+\infty} (s - x)^{1-\alpha} U(s, y, t) ds, \end{aligned}$$

where $\Gamma(\cdot)$ is the Gamma function.

3 Stability and bifurcation analysis in the non-diffusion model

The prerequisite for studying the spatiotemporal dynamic characteristics in model (2) is to have a comprehensive understanding of the dynamics in the non-diffusion model (2). Therefore, this section investigates the stability and bifurcation analysis in the non-diffusion model (2). First, through calculations, we find that model (2) has three equilibria, which are trivial equilibrium $E_0 = (0, 0)$, semi-trivial equilibrium $E_1 = (1, 0)$, and a coexistence equilibrium $E_* = (U_*, V_*)$ with $U_* = \frac{\gamma}{\beta(1-\gamma)}$ and $V_* = \frac{\beta(1-\gamma)-\gamma}{\beta(1-\gamma)^2}$, which is positive when $\beta > \frac{\gamma}{1-\gamma}$ and $\gamma < 1$.

3.1 Stability of equilibria

Next, we provide stability analysis by calculating the eigenvalues of the Jacobian matrix in the non-diffusion model (2). Let

$$\begin{aligned} f(U, V) &= AU \left[(1 - U) - \frac{V}{1 + \beta U} \right], \\ g(U, V) &= V \left(\frac{\beta U}{1 + \beta U} - \gamma \right). \end{aligned}$$

The Jacobian matrix J for non-diffusion model (2) is

$$J = \begin{pmatrix} \frac{\partial f}{\partial U} & \frac{\partial f}{\partial V} \\ \frac{\partial g}{\partial U} & \frac{\partial g}{\partial V} \end{pmatrix}, \quad (3)$$

where

$$\begin{aligned} \frac{\partial f}{\partial U} &= A \left[(1 - U) - \frac{V}{1 + \beta U} + U \left(\frac{\beta V}{(1 + \beta U)^2} - 1 \right) \right], \quad \frac{\partial f}{\partial V} = AU \left(-\frac{1}{1 + \beta U} \right), \\ \frac{\partial g}{\partial U} &= V \left(\frac{\beta(1 + \beta U) - \beta U \cdot \beta}{(1 + \beta U)^2} \right) = V \left(\frac{\beta}{(1 + \beta U)^2} \right), \quad \frac{\partial g}{\partial V} = \frac{\beta U}{1 + \beta U} - \gamma. \end{aligned}$$

Theorem 1 *Regarding the non-diffusion model (2), the following results are obtained.*

- (i) *trivial equilibrium $E_0 = (0, 0)$ is always a saddle point.*
- (ii) *If $\beta < \frac{\gamma}{1-\gamma}$, there is no positive equilibrium and semi-trivial equilibrium $E_1 = (1, 0)$ is a stable node point. If $\beta > \frac{\gamma}{1-\gamma}$, then semi-trivial equilibrium $E_1 = (1, 0)$ is a saddle point.*
- (iii) *If $\beta > \frac{1+\gamma}{1-\gamma}$, then $E_* = (U_*, V_*)$ is unstable node point. If $\frac{\gamma}{1-\gamma} < \beta < \frac{1+\gamma}{1-\gamma}$, then $E_* = (U_*, V_*)$ is stable node point. When $\beta = \frac{1+\gamma}{1-\gamma}$, the stability of E_* remains unknown without a center manifold reduction.*

Proof Evaluating the Jacobian matrix for the non-diffusion model (2) at $E_0 = (0, 0)$, we find

$$J_0 = \begin{pmatrix} A & 0 \\ 0 & -\gamma \end{pmatrix}. \quad (4)$$

It can be calculated that $E_0 = (0, 0)$ is always a saddle point.

Evaluating the Jacobian matrix for the non-diffusion model (2) at $E_1 = (1, 0)$, we find

$$J_1 = \begin{pmatrix} -A & -\frac{A}{1+\beta} \\ 0 & \frac{\beta}{1+\beta} - \gamma \end{pmatrix}, \quad (5)$$

the characteristic polynomial is

$$H_1(\lambda) = \lambda^2 - \left(\frac{\beta}{1+\beta} - \gamma - A \right) \lambda - A \left(\frac{\beta}{1+\beta} - \gamma \right). \quad (6)$$

If $\beta < \frac{\gamma}{1-\gamma}$, there is no positive equilibrium and semi-trivial equilibrium $E_1 = (1, 0)$ is a stable node point. If $\beta > \frac{\gamma}{1-\gamma}$, then semi-trivial equilibrium $E_1 = (1, 0)$ is a saddle point.

The Jacobian matrix for the non-diffusion model (2) evaluated at $E_* = (U_*, V_*)$ is given by

$$J_* = \begin{pmatrix} a_{10} & a_{01} \\ b_{10} & b_{01} \end{pmatrix}, \quad (7)$$

where

$$a_{10} = \frac{A\gamma(\beta - \frac{1+\gamma}{1-\gamma})}{\beta}, \quad a_{01} = -\frac{A\gamma}{\beta}, \quad b_{10} = \beta(1 - \gamma) - \gamma, \quad b_{01} = 0.$$

The characteristic polynomial is

$$\lambda^2 - Tr_0\lambda + Det_0 = 0,$$

here

$$Tr_0 = a_{10} + b_{01} = \frac{A\gamma(\beta - \frac{1+\gamma}{1-\gamma})}{\beta}, \quad (8)$$

$$Det_0 = (a_{10}b_{01} - a_{01}b_{10}) = A\gamma \left[(1 - \gamma) - \frac{\gamma}{\beta} \right].$$

If $\beta > \frac{\gamma}{1-\gamma}$ and $\gamma < 1$, then $Det_0 > 0$. Under this scenario, we need to discuss the positive or negative property of Tr_0 . If $\beta > \frac{1+\gamma}{1-\gamma}$, then $Tr_0 > 0$ that means $E_* = (U_*, V_*)$ is unstable. If $\frac{\gamma}{1-\gamma} < \beta < \frac{1+\gamma}{1-\gamma}$, then $Tr_0 < 0$ that means $E_* = (U_*, V_*)$ is stable. When $\beta = \frac{1+\gamma}{1-\gamma}$, the stability of E_* remains unknown without a center manifold reduction. The proof of the theorem is completed. \square

Further, we have rigorously proven the global asymptotic stability of the semi-trivial equilibrium E_1 and coexistence (positive) equilibrium E_* on non-diffusion model (2) by employing Lyapunov functions, as demonstrated in Theorems 2 and 3.

Theorem 2 Assume that $0 < \beta < \gamma$, then the semi-trivial equilibrium $E_1 = (U_1, V_1) = (1, 0)$ of non-diffusion model (2) is globally asymptotically stable.

Proof Consider the Lyapunov function:

$$L_1(U, V) = \int_{U_1}^U \frac{P - U_1}{P} dP + \frac{A}{\beta} \int_{V_1}^V 1 dQ. \quad (9)$$

The derivative of $L_1(U, V)$ along the solution of non-diffusion model (2) is

$$\begin{aligned} \frac{dL_1}{dt} &= \frac{U - 1}{U} \frac{dU}{dt} + \frac{A}{\beta} \frac{dV}{dt} \\ &= A(U - 1) \left[(1 - U) - \frac{V}{1 + \beta U} \right] + \frac{A}{\beta} V \left(\frac{\beta U}{1 + \beta U} - \gamma \right) \\ &= A \left(-(U - 1)^2 - \frac{V(U - 1)}{1 + \beta U} + \frac{UV}{1 + \beta U} - \frac{\gamma}{\beta} V \right) \\ &= A \left(-(U - 1)^2 - \frac{UV}{1 + \beta U} + \frac{V}{1 + \beta U} + \frac{UV}{1 + \beta U} - \frac{\gamma}{\beta} V \right) \\ &= A \left(-(U - 1)^2 + \frac{1}{1 + \beta U} V - \frac{\gamma}{\beta} V \right). \end{aligned}$$

If $0 < \beta < \gamma$, then $\frac{dL}{dt} < 0$, so $E_1 = (1, 0)$ is globally stable for all $U, V > 0$ and $L_1(1, 0) = 0$. The proof of the theorem is completed. \square

Theorem 3 Assume that $\frac{\gamma}{1-\gamma} < \beta < \frac{1}{1-\gamma}$, then the coexistence (positive) equilibrium $E_* = (U_*, V_*)$ of non-diffusion model (2) is globally asymptotically stable in the positive invariant set.

Proof Consider the Lyapunov function:

$$L(U, V) = U - U_* - U_* \ln \left(\frac{U}{U_*} \right) + p \left[V - V_* - V_* \ln \left(\frac{V}{V_*} \right) \right] (p > 0). \quad (10)$$

The derivative of $L(U, V)$ along the solution of non-diffusion model (2) is

$$\begin{aligned} \frac{dL}{dt} &= \frac{U - U_*}{U} \frac{dU}{dt} + p \frac{V - V_*}{V} \frac{dV}{dt} \\ &= A(U - U_*) \left[(1 - U) - \frac{V}{1 + \beta U} \right] + p(V - V_*) \left(\frac{\beta U}{1 + \beta U} - \gamma \right) \\ &= A(U - U_*) \left[(U_* - U) + \frac{V_*}{1 + \beta U_*} - \frac{V}{1 + \beta U} \right] \\ &\quad + p(V - V_*) \left(\frac{\beta U}{1 + \beta U} - \frac{\beta U_*}{1 + \beta U_*} \right) \\ &= A(U - U_*) \left[-(U - U_*) + \frac{V_* + \beta UV_* - V - \beta VU_*}{(1 + \beta U_*)(1 + \beta U)} \right] \\ &\quad + p(V - V_*) \left(\frac{\beta(U - U_*)}{(1 + \beta U_*)(1 + \beta U)} \right) \end{aligned}$$

$$\begin{aligned}
&= A(U - U_*) \left[-(U - U_*) - \frac{V - V_*}{(1 + \beta U_*)(1 + \beta U)} \right. \\
&\quad \left. + \frac{\beta [UV_* - U_*V_* + U_*V_* - U_*V]}{(1 + \beta U_*)(1 + \beta U)} \right] \\
&\quad + p \left(\frac{\beta(U - U_*)(V - V_*)}{(1 + \beta U_*)(1 + \beta U)} \right) \\
&= -A(U - U_*)^2 - \frac{A(V - V_*)(U - U_*)}{(1 + \beta U_*)(1 + \beta U)} + \frac{A\beta V_*(U - U_*)^2}{(1 + \beta U_*)(1 + \beta U)} \\
&\quad - \frac{A\beta U_*(V - V_*)(U - U_*)}{(1 + \beta U_*)(1 + \beta U)} \\
&\quad + p \left(\frac{\beta(U - U_*)(V - V_*)}{(1 + \beta U_*)(1 + \beta U)} \right) \\
&= -A(U - U_*)^2 \left(1 - \frac{\beta V_*}{(1 + \beta U_*)(1 + \beta U)} \right) \\
&\quad + \frac{(-A - A\beta U_* + p\beta)(V - V_*)(U - U_*)}{(1 + \beta U_*)(1 + \beta U)}.
\end{aligned}$$

By using $p = \frac{A+A\beta U_*}{\beta}$ and value of (U_*, V_*) , one obtains

$$\begin{aligned}
\frac{dL}{dt} &= -A(U - U_*)^2 \left(1 - \frac{\beta V_*}{(1 + \beta U_*)(1 + \beta U)} \right) \\
&= \frac{-A(U - U_*)^2}{(1 + \beta U_*)(1 + \beta U)} [(1 + \beta U_*)(1 + \beta U) - \beta V_*] \\
&\leq \frac{-A(U - U_*)^2}{(1 + \beta U_*)(1 + \beta U)} (1 + \beta U_* - \beta V_*) \\
&\leq \frac{-A(U - U_*)^2}{(1 + \beta U_*)(1 + \beta U)} \left(1 + \frac{\gamma}{(1 - \gamma)} - \frac{\beta(1 - \gamma) - \gamma}{(1 - \gamma)^2} \right)
\end{aligned}$$

If $\frac{\gamma}{1-\gamma} < \beta < \frac{1}{1-\gamma}$, then $\frac{dL}{dt} < 0$, so $E_* = (U_*, V_*)$ is globally stable for all $U, V > 0$ and $L(U_*, V_*) = 0$. The proof of the theorem is completed. \square

3.2 Bifurcation analysis

In this subsection, we delve into the existence of bifurcations around equilibria, considering the parameter β as the bifurcation parameter while holding all other parameters constant. To investigate the onset and specify the nature of bifurcations, we employ Sotomayor's bifurcation theorem [31].

Theorem 4 Non-diffusion model (2) undergoes a transcritical bifurcation around the semi-trivial equilibrium E_1 at $\beta = \beta_T$, where $\beta_T = \frac{\gamma}{1-\gamma}$.

Proof If $\text{Det}(J_1) = 0$, i.e. $\beta = \beta_T$, then one of the eigenvalues of J_1 is zero. In this case, another eigenvalue is $-A$. If \mathcal{V} and W represent eigenvectors corresponding to eigenvalues 0 of matrices J_1 and J_1^T , respectively, we obtain $\mathcal{V} = (\frac{-1}{1+\beta}, 1)^T$ and $W = (0, 1)^T$, where $J_1^T = \begin{pmatrix} -A & 0 \\ -\frac{A}{1+\beta} & 0 \end{pmatrix}$, $\mathcal{V}_1 = \frac{-1}{1+\beta}$, $\mathcal{V}_2 = 1$.

$$\begin{aligned} W^T \begin{pmatrix} f_\beta(E_1, \beta_T) \\ g_\beta(E_1, \beta_T) \end{pmatrix} &= (0, 1) \left(\begin{pmatrix} \frac{\partial f(U, V)}{\partial \beta} \\ \frac{\partial g(U, V)}{\partial \beta} \end{pmatrix} \right)_{E_1} = (0, 1) \begin{pmatrix} 0 \\ 0 \end{pmatrix} = 0, \\ W^T \left[\begin{pmatrix} Df_\beta(E_1, \beta_T) \\ Dg_\beta(E_1, \beta_T) \end{pmatrix} \mathcal{V} \right] &= (0, 1) \left(\begin{pmatrix} \frac{\partial^2 f(U, V)}{\partial U \partial \beta} & \frac{\partial^2 f(U, V)}{\partial V \partial \beta} \\ \frac{\partial^2 g(U, V)}{\partial U \partial \beta} & \frac{\partial^2 g(U, V)}{\partial V \partial \beta} \end{pmatrix} \right)_{E_1} \begin{pmatrix} \frac{-1}{1+\beta} \\ 1 \end{pmatrix} \\ &= (0, 1) \begin{pmatrix} 0 - A(1-\gamma)^2 \\ 0 - (1-\gamma)^2 \end{pmatrix} \begin{pmatrix} \frac{-1}{1+\beta} \\ 1 \end{pmatrix} = (1-\gamma)^2 \neq 0, \\ W^T \left[\begin{pmatrix} D^2 f(E_1, \beta_T) \\ D^2 g(E_1, \beta_T) \end{pmatrix} (\mathcal{V}, \mathcal{V}) \right] &= W^T \left(\begin{pmatrix} \frac{\partial^2 f(U, V)}{\partial U^2} \mathcal{V}_1^2 + 2 \frac{\partial^2 f(U, V)}{\partial U \partial V} \mathcal{V}_1 \mathcal{V}_2 + \frac{\partial^2 f(U, V)}{\partial V^2} \mathcal{V}_2^2 \\ \frac{\partial^2 g(U, V)}{\partial U^2} \mathcal{V}_1^2 + 2 \frac{\partial^2 g(U, V)}{\partial U \partial V} \mathcal{V}_1 \mathcal{V}_2 + \frac{\partial^2 g(U, V)}{\partial V^2} \mathcal{V}_2^2 \end{pmatrix}_{E_1} \right. \\ &= (0, 1) \begin{pmatrix} -2A\mathcal{V}_1^2 - A(1-\gamma)^2 \mathcal{V}_1 \mathcal{V}_2 \\ \gamma(1-\gamma) \mathcal{V}_1 \mathcal{V}_2 \end{pmatrix} \\ &= \frac{-\gamma(1-\gamma)}{1+\beta} \neq 0. \end{aligned}$$

Therefore, by the Sotomayor theorem [31], we can find that non-diffusion model (2) experiences transcritical bifurcation at $\beta = \beta_T$ around the semi-trivial equilibrium E_1 . \square

Theorem 5 (i) The non-diffusion model (2) undergoes a Hopf bifurcation at E_* when the following conditions are satisfied:

$$Tr_0(\beta_H) = 0, \quad \text{Det}_0 > 0, \quad \left. \frac{dTr_0(\beta)}{d\beta} \right|_{\beta=\beta_H} > 0,$$

where $\beta_H = \frac{1+\gamma}{1-\gamma}$.

- (ii) If $l_1 < 0$, then the Hopf bifurcation is supercritical and the bifurcation periodic solution from E_* is stable; if $l_1 > 0$, then the Hopf bifurcation is subcritical and the bifurcation periodic solution is unstable.

Proof Next, we prove that the non-diffusion model (2) undergoes a Hopf bifurcation if $\beta = \frac{1+\gamma}{1-\gamma}$. Denote $\beta_H = \frac{1+\gamma}{1-\gamma}$, when $\beta = \beta_H$, we have $Tr_0 = 0$. The Jacobian matrix J_* has a pair of imaginary eigenvalues $\lambda = \pm i\sqrt{\text{Det}_0}$. Let $\lambda = \eta(\beta) \pm \omega(\beta)i$ be the roots of $\lambda^2 - Tr_0\lambda + \text{Det}_0 = 0$, then

$$\begin{aligned} \eta^2 - \omega^2 - \eta Tr_0 + \text{Det}_0 &= 0, \\ 2\eta\omega - Tr_0\omega &= 0, \end{aligned}$$

and

$$\eta = \frac{Tr_0}{2}, \quad \omega = \frac{\sqrt{4\text{Det}_0 - Tr_0^2}}{2},$$

$$\left. \frac{d\eta(\beta)}{d\beta} \right|_{\beta=\beta_H} = \frac{A\gamma(1-\gamma)}{2(1+\gamma)} > 0.$$

According to the Hopf bifurcation theorem, we know that non-diffusion model (2) undergoes a Hopf bifurcation at $E_* = (U_*, V_*)$ when $\beta = \beta_H$. However, the detailed nature of the Hopf bifurcation needs further analysis of the normal form of non-diffusion model (2). We determine the direction of the Hopf bifurcation by calculating the first Lyapunov number. Set $u = U - U_*$ and $v = V - V_*$, to (U_*, V_*) as the origin of co-ordinates (u, v) . We have the following system

$$\begin{aligned}\frac{du}{dt} &= a_{10}u + a_{01}v + F(u, v), \\ \frac{dv}{dt} &= b_{10}u + b_{01}v + G(u, v),\end{aligned}$$

where

$$\begin{aligned}F(u, v) &= a_{20}u^2 + a_{11}uv + a_{02}v^2 + a_{30}u^3 + a_{21}u^2v + a_{12}uv^2 + a_{03}v^3 + P_1(u, v), \\ G(u, v) &= b_{20}u^2 + b_{11}uv + b_{02}v^2 + b_{30}u^3 + b_{21}u^2v + b_{12}uv^2 + b_{03}v^3 + P_2(u, v),\end{aligned}$$

and

$$\begin{aligned}a_{20} &= A \left(-1 + \frac{V_*\beta}{(\beta U_* + 1)^2} \right) - \frac{AU_*V_*\beta^2}{(\beta U_* + 1)^3}, \\ a_{11} &= -\frac{A}{\beta U_* + 1} + \frac{AU_*\beta}{(\beta U_* + 1)^2}, \quad a_{02} = 0, \\ b_{20} &= V_* \left(-\frac{\beta^2}{(\beta U_* + 1)^2} + \frac{\beta^3 U_*}{(\beta U_* + 1)^3} \right), \\ b_{11} &= \frac{\beta}{\beta U_* + 1} - \frac{\beta^2 U_*}{(\beta U_* + 1)^2}, \quad b_{02} = 0, \\ a_{30} &= -\frac{AV_*\beta^2}{(\beta U_* + 1)^3} + \frac{AU_*V_*\beta^3}{(\beta U_* + 1)^4}, \\ a_{21} &= \frac{A\beta}{(\beta U_* + 1)^2} - \frac{AU_*\beta^2}{(\beta U_* + 1)^3}, \quad a_{12} = 0, \quad a_{03} = 0, \\ b_{30} &= V_* \left(\frac{\beta^3}{(\beta U_* + 1)^3} - \frac{\beta^4 U_*}{(\beta U_* + 1)^4} \right), \\ b_{21} &= -\frac{\beta^2}{(\beta U_* + 1)^2} + \frac{\beta^3 U_*}{(\beta U_* + 1)^3}, \quad b_{12} = 0, \quad b_{03} = 0,\end{aligned}$$

where $P_1(u, v)$, $P_2(u, v)$ are smooth functions of u and v at least of order four. To obtain the direction and stability of Hopf bifurcation, it is necessary to calculate the

Lyapunov coefficient l_1 :

$$\begin{aligned} l_1 = & \frac{-3\pi}{2a_{01}\Delta^{\frac{3}{2}}} \{ [a_{10}b_{01}(a_{11}^2 + a_{11}b_{02} + a_{02}b_{11}) + a_{10}a_{01}(b_{11}^2 + b_{11}a_{02} + b_{02}a_{11}) \\ & + b_{10}^2(a_{11}a_{02} + 2a_{02}b_{02}) - 2a_{10}b_{10}(b_{02}^2 - a_{20}a_{02}) - 2a_{10}a_{01}(a_{20}^2 - b_{20}b_{02}) \\ & - a_{01}^2(2a_{20}b_{20} + b_{11}b_{20}) + (a_{01}b_{10} - 2a_{10}^2)(b_{11}b_{02} - a_{11}a_{20})] \\ & - (a_{10}^2 + a_{01}b_{10})[3(b_{10}b_{03} - a_{01}a_{30}) + 2a_{10}(a_{21} + b_{12}) + (b_{10}a_{12} - a_{01}b_{21})] \}, \end{aligned} \quad (11)$$

where

$$\Delta = \frac{A\gamma [\beta(1-\gamma) - \gamma]}{\beta}.$$

If $l_1 < 0$, then the Hopf bifurcation is supercritical and the bifurcation periodic solution from E_* is stable; if $l_1 > 0$, then the Hopf bifurcation is subcritical and the bifurcation periodic solution is unstable. \square

3.3 Example

In this subsection, we provide some numerical examples to illustrate the previous trivial equilibrium $E_0 = (0, 0)$, semi-trivial equilibrium $E_1 = (1, 0)$, and coexistence (positive) equilibrium $E_* = (U_*, V_*)$. Here, the parameters are $A = 0.25$ and $\gamma = 0.45$. Therefore, non-diffusion model (2) is in the following form:

$$\begin{cases} \frac{dU}{dT} = AU \left[(1-U) - \frac{V}{1+\beta U} \right], \\ \frac{dV}{dT} = V \left(\frac{\beta U}{1+\beta U} - \gamma \right). \end{cases} \quad (12)$$

Based on the abovementioned analysis of Theorems 1 and 4, as well as Hopf bifurcation. The phase portraits and bifurcation diagram of the numerical example (12) are shown in Fig. 1.

Remark 1 The stability of the limit cycle presented in Fig. 1 is established based on our computation of the first Lyapunov number. Our calculations reveal that, for the selected parameters $A = 0.25$, $\beta = 3$, and $\gamma = 0.45$, the value of l_1 is -23.7619 , which is less than zero. Consequently, the Hopf bifurcation is determined to be supercritical, and the bifurcating periodic solution emanating from E_* is stable.

4 Hopf bifurcation and spatiotemporal pattern in spatial fractional model

Pattern formation in reaction-diffusion systems typically arises from two instability mechanisms: Turing (spatial) and Hopf (temporal) bifurcations [32]. In this study, we rigorously demonstrate that Turing instability cannot occur in the model (2). This absence shifts the focus to Hopf bifurcation as the sole pathway for spatiotemporal pattern generation. This section achieves two goals:

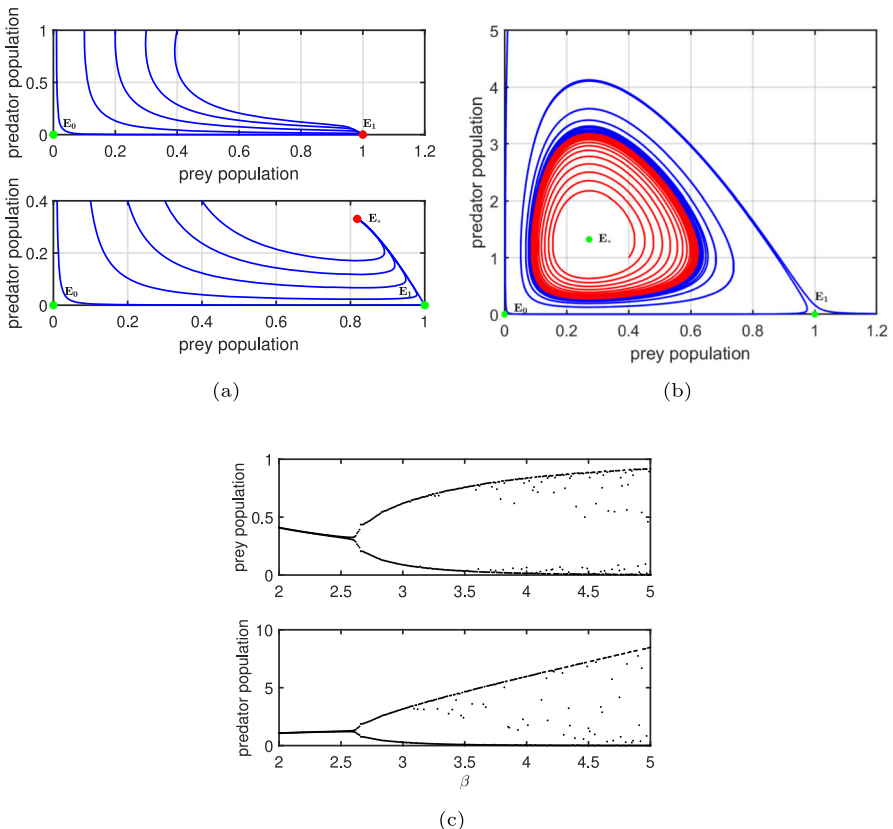


Fig. 1 In Panel (a), the results indicate that for $\beta = 0.8 < \beta_T$, E_0 exhibits the characteristics of a saddle point, while E_1 manifests as a stable node. Conversely, when $\beta = 1 > \beta_T$, both E_0 and E_1 transition into saddle points, with E_* assuming the role of a stable node. Panel (b) presents the $\beta = 3 > \beta_H$ findings. In this scenario, both E_0 and E_1 continue to function as saddle points, whereas E_* becomes an unstable node, accompanied by the emergence of a stable limit cycle. Finally, Panel (c) features a bifurcation diagram, where β serves as the bifurcation parameter

- **Exclusion of Turing patterns:** By proving that the determinant condition $\text{Det}_k > 0$ holds for all $k \neq 0$, we confirm the system's inability to form static Turing structures.
- **Characterization of Hopf-driven patterns:** We show that Hopf bifurcation, when coupled with fractional diffusion, generates wave patterns instead of static Turing patterns. These waves emerge through synchronization of local oscillations, with wavelengths modulated by the fractional order α .

Our analysis bridges classical bifurcation theory with anomalous transport effects, offering new principles for pattern control in systems where Turing mechanisms are inactive.

4.1 Hopf bifurcation in spatial fractional model

To analyze Hopf bifurcation around positive equilibrium $E_* = (U_*, V_*)$, one translates it to the origin point by taking the change of coordinate in the form

$$\mathbf{W}(T) = \begin{pmatrix} \bar{U}(T) \\ \bar{V}(T) \end{pmatrix} = \begin{pmatrix} U(T) - U_* \\ V(T) - V_* \end{pmatrix}. \quad (13)$$

For the sake of convenience, we still denote $\bar{U}(T)$ and $\bar{V}(T)$ by $U(T)$ and $V(T)$. Model (2) is then rewritten as

$$\mathbf{W}_t = \mathbf{D}\nabla^\alpha \mathbf{W} + J_* \mathbf{W} + H.O.T.,$$

where *H.O.T.* for the shorthand of “higher order terms” and

$$\mathbf{D} = \begin{pmatrix} D_U & 0 \\ 0 & D_V \end{pmatrix}, \quad J_* = \begin{pmatrix} a_{10} & a_{01} \\ b_{10} & b_{01} \end{pmatrix},$$

$$a_{10} = \frac{A\gamma(\beta - \frac{1+\gamma}{1-\gamma})}{\beta}, \quad a_{01} = -\frac{A\gamma}{\beta}, \quad b_{10} = \beta(1-\gamma) - \gamma, \quad b_{01} = 0.$$

So, the linearization form of the model is as follows

$$\begin{pmatrix} \frac{\partial U}{\partial T} \\ \frac{\partial V}{\partial T} \end{pmatrix} = \mathbf{D} \begin{pmatrix} \nabla^\alpha U \\ \nabla^\alpha V \end{pmatrix} + J_* \begin{pmatrix} U \\ V \end{pmatrix}. \quad (14)$$

To analyze the stability of coexistence (positive) equilibrium $E_* = (U_*, V_*)$, assume that model (2) has a general solution as follows:

$$\begin{pmatrix} U \\ V \end{pmatrix} = \begin{pmatrix} c_1 \\ c_2 \end{pmatrix} \exp(\lambda T + ik \cdot \mathbf{x}). \quad (15)$$

Here, λ represents the rate of growth of the perturbation over time T . i is the imaginary unit, satisfying $i^2 = -1$. k is the wave vector, and \mathbf{x} is the spatial vector. Consequently, we can deduce the following characteristic equation:

$$\lambda^2 - Tr_k \lambda + Det_k = 0, \quad \forall k \in \mathbb{N}, \quad (16)$$

here

$$Tr_k = a_{10} + b_{01} - (D_U + D_V)k^\alpha,$$

$$Det_k = D_U D_V k^{2\alpha} - (a_{10} D_V + b_{01} D_U)k^\alpha + (a_{10} b_{01} - a_{01} b_{10}). \quad (17)$$

We can divide the discussion of stability into two categories:

- (1) $Tr_k > 0$ and $Det_k > 0$, which means that the equilibrium $E_* = (U_*, V_*)$ becomes unstable. More specifically, we choose β as the control parameter and let $\beta_H = \frac{1+\gamma}{1-\gamma}$, $\beta_{H_k} = \frac{1+\gamma}{1-\gamma} \frac{A\gamma}{A\gamma - (D_U + D_V)k^\alpha}$. If $\beta < \beta_H$, then the equilibrium $E_* = (U_*, V_*)$

is stable without diffusion, and its stability will not change because of $k^\alpha > 0$. If $\beta > \beta_{H_k}$, then the equilibrium $E_* = (U_*, V_*)$ is unstable.

(2) Following the classical Turing theory, two conditions must hold:

- **Homogeneous stability:** The steady state must be stable under spatially homogeneous perturbations ($k = 0$). For our model, this is ensured by $Tr_k < 0$ (equivalent to $a_{10} + b_{01} < 0$).
- **Instability for nonzero modes:** There must exist some $k \neq 0$ where the steady state becomes unstable (i.e., $Det_k < 0$).

However, in our model, $a_{10} < 0$ and $b_{01} = 0$, leading to $Det_k = (a_{10} - D_U k^\alpha)(-D_V k^\alpha) - a_{01}b_{10}$. Since $a_{10} - D_U k^\alpha < 0$ (due to $a_{10} < 0$ and $k^\alpha > 0$) and $D_V k^\alpha > 0$, the term $(a_{10} - D_U k^\alpha)(-D_V k^\alpha)$ is positive. Combined with $-a_{01}b_{10} > 0$, Det_k remains positive for all $k \neq 0$, thereby precluding Turing instability.

In summary, when $Det_k > 0$, we can find that if we want $E_* = (U_*, V_*)$ to become unstable, only condition $\beta > \beta_{H_k}$ is satisfied. Furthermore, when $\beta = \beta_{H_k}$, a purely imaginary root $\pm\sqrt{Det_k}i$. Now, to verify the transversality condition of the Hopf bifurcation, take β as a parameter and let $\lambda(\beta)$ be the root of Eq. (16), then

$$\left. \frac{d \operatorname{Re} \lambda(\beta)}{d\beta} \right|_{\beta=\beta_{H_k}} = \frac{A\gamma(1+\gamma)}{2\beta_{H_k}^2(1-\gamma)} > 0. \quad (18)$$

Therefore, we can prove that model (2) undergoes a Hopf bifurcation around positive equilibrium $E_* = (U_*, V_*)$ when $\beta = \beta_{H_k}$.

4.2 2D and 3D spatiotemporal patterns

In this subsection, we endeavor to capture specific patterns via computer simulation, utilizing a detailed numerical simulation method derived from [33]. For a two-dimensional domain $(x, y) \in \Omega = (0, 400) \times (0, 400)$, we adopt a spatial step size of $\Delta x = 1$, a temporal step size of $\Delta T = 1$, and a total simulation time of $T = 50000$. To simulate 2D and 3D patterns of the model given by (2), we perform time discretization, yielding:

$$\begin{cases} \frac{U^{n+1,m} - U^n}{\Delta T} = -D_U(-\Delta)^{\alpha/2}U^{n+1,m} + f(U^{n+1,m-1}, V^{n+1,m-1}, T^{n+1}), \\ \frac{V^{n+1,m} - V^n}{\Delta T} = -D_V(-\Delta)^{\alpha/2}V^{n+1,m} + g(U^{n+1,m-1}, V^{n+1,m-1}, T^{n+1}). \end{cases} \quad (19)$$

Within each time step $[T_n, T_{n+1}]$, we employ the following fixed-point iteration to handle the nonlinear term: given U^n , we define $U^{n+1,0} := U^n$ and seek $U^{n+1,m}$ for $m = 1, 2, \dots, l$. When $l = 1$, the nonlinear term is treated explicitly. For sufficiently large l , the method becomes entirely implicit. By applying the Fourier transform to both sides of Eq. (19) and utilizing the definition of the fractional Laplace operator

given below,

$$\nabla^\alpha U(x) = - \sum_{j=0}^{\infty} \widehat{U}_j \lambda_j^{\frac{\alpha}{2}} \varphi_j, \quad U \in I_\alpha,$$

where $I_\alpha := \left\{ U = \sum_{j=0}^{\infty} \widehat{U}_j \varphi_j, \quad \widehat{U}_j = \langle U, \varphi_j \rangle, \quad \sum_{j=0}^{\infty} |\widehat{U}_j|^2 |\lambda_j|^{\frac{\alpha}{2}} < \infty \right\}$, with λ_j and φ_j being the eigenvalues and orthogonal eigenfunctions of the standard Laplace operator ∇^2 , respectively, satisfying the standard boundary condition on the bounded domain $\Omega \subset \mathbb{R}^n$, i.e., $\nabla^2 \varphi_j = -\lambda_j \varphi_j$. We obtain the spatiotemporal discretization form for the j -th Fourier mode:

$$\begin{cases} \frac{\widehat{U}^{n+1,m} - \widehat{U}^n}{\Delta T} = -D_U \lambda_j^{\alpha/2} \widehat{U}^{n+1,m} + \widehat{f}_j \left(\widehat{U}^{n+1,m-1}, \widehat{V}^{n+1,m-1}, T^{n+1} \right), \\ \frac{\widehat{V}^{n+1,m} - \widehat{V}^n}{\Delta T} = -D_V \lambda_j^{\alpha/2} \widehat{V}^{n+1,m} + \widehat{g}_j \left(\widehat{U}^{n+1,m-1}, \widehat{V}^{n+1,m-1}, T^{n+1} \right), \end{cases} \quad (20)$$

where \widehat{f}_j and \widehat{g}_j represent the j -th Fourier coefficients of the first and second reaction terms, respectively, with each Fourier coefficient independent of the others.

The selection of its parameters and initial values will be given in each group of figure captions. When we fix the parameters $A = 0.3$ and $\gamma = 0.5$, it is easy to calculate the critical value parameter $\beta_H = 3$ that undergoes Hopf bifurcation. Furthermore, when we set the control parameter to $\beta = 2 < \beta_H$, the positive equilibrium $E_* = (0.5, 1)$ is stable. As shown in Fig. 2 (a), (d), and (g), regardless of whether we consider diffusion or adjust the initial value, the stable equilibrium state will not change. However, when we set $\beta = 5$ or $\beta = 12$, model (2) exhibits periodic or irregular oscillation as shown in Fig. 2 (b), (c), (e), (f), (h), and (i). It is worth noting that when the initial value is set to $(U_0, V_0) = (U_*, V_*) + 0.0001 \times \text{rand}(0, 1)$ and random small perturbations are generated using “rand” function, the temporal periodic oscillations of prey and predator species density are almost consistent with those of model (2) without diffusion (please see Fig. 2 (b), (c), (e), and (f)). However, when we change the initial value to $(U_0, V_0) = (U_*, V_*) + 0.0001 \times (1, 1)$ if $(x - 200)^2 + (y - 200)^2 < 20000$ otherwise $(U_0, V_0) = (U_*, V_*)$, irregular oscillations occur (see Fig. 2 (h) and (i)).

Consequently, we have the concern that since the average species density at different locations in the region exhibits irregular oscillations over time, is the oscillation of species density at each location consistent over time? If inconsistent, will it self-organize and form phase waves after coupling with diffusion, resulting in some specific spatiotemporal patterns? To answer these questions, we keep the selection of initial values consistent with Fig. 2 and find the presence of symmetric spiral patterns and concentric waves. Moreover, the switching between concentric waves and spiral patterns is influenced by fractional order (see Fig. 3), indicating the importance of fractional order in controlling spatial patterns. Considering the particularity of initial value selection, we attempted another asymmetric initial value $((U_0, V_0) = (U_*, V_*) + 0.0002 \times (1, 1)$ if $(x - 300)^2 + (y - 100)^2 < 20000$ and $(x - 100)^2 + (y - 300)^2 < 10000$, $(U_0, V_0) = (U_*, V_*)$ if $(x - 300)^2 + (y - 100)^2 \geq 20000$ and $(x - 100)^2 + (y - 300)^2 \geq 10000$, otherwise $(U_0, V_0) = (U_*, V_*) + 0.0001 \times (1, 1)$). Similar to the symmetric initial value, where the spiral pattern was captured. However, concentric waves disappear

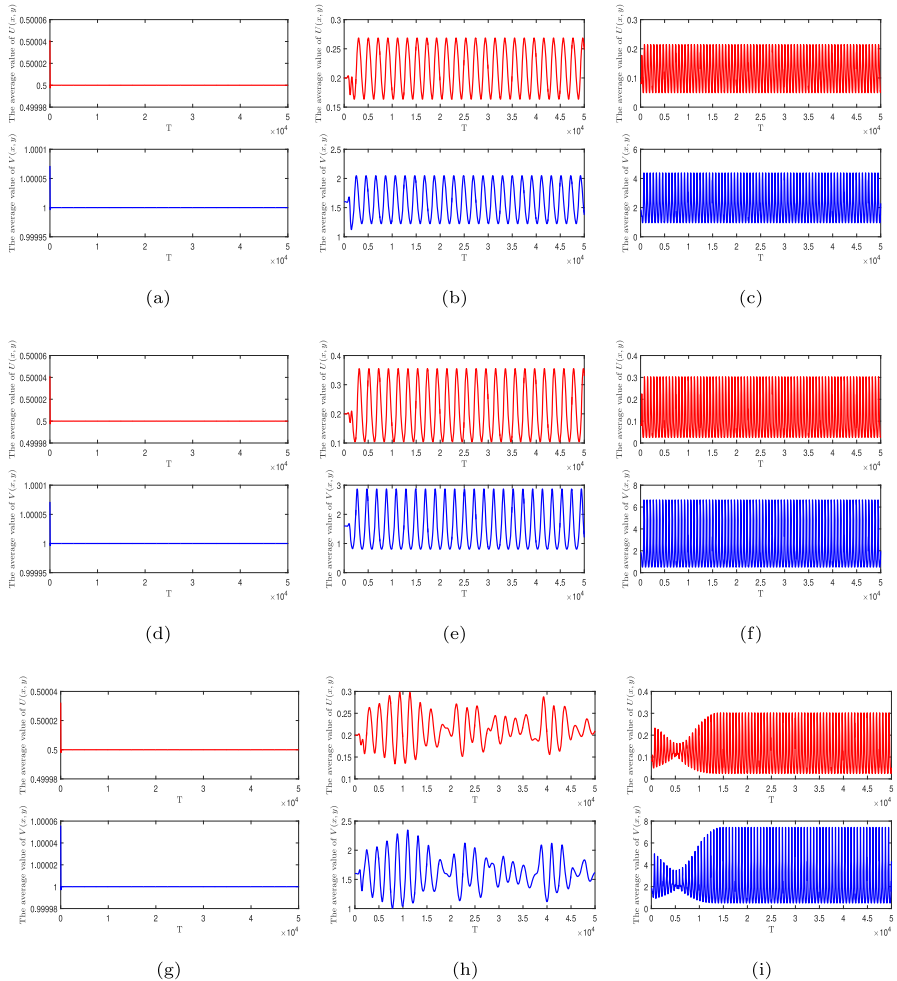


Fig. 2 The evolution of the average density of prey (U) and predator (V) species at different locations (x, y) over time (T). **(a)** $\beta = 2$, **(b)** $\beta = 5$, and **(c)** $\beta = 12$ for model (2) without diffusion; **(d)** $\beta = 2$, **(e)** $\beta = 5$, and **(f)** $\beta = 12$ for model (2) with diffusion and initial value is $(U_0, V_0) = (U_*, V_*) + 0.0001 \times \text{rand}(0, 1)$; **(g)** $\beta = 2$, **(h)** $\beta = 5$, and **(i)** $\beta = 12$ for model (2) with diffusion and initial value is $(U_0, V_0) = (U_*, V_*) + 0.0001 \times (1, 1)$ if $(x - 200)^2 + (y - 200)^2 < 20000$, otherwise $(U_0, V_0) = (U_*, V_*)$. Other parameters are: $D_U = 0.01$, $D_V = 0.05$, $A = 0.3$, $\alpha = 1.5$, and $\gamma = 0.5$. Interestingly, we capture beautiful spatiotemporal patterns, namely spiral patterns, under the parameters of panel **(h)** and **(i)**. However, no specific pattern is formed when the initial value is small perturbations around the positive equilibrium

under the same parameters, and we believe that concentric waves are greatly affected by their initial values. Interestingly, the spiral pattern's patch area increases with the fractional order decrease, which is also well demonstrated in Fig. 4.

Nagano and Maeda point out that as the control parameter (β) and difference in diffusion coefficients ($D_U = 0.01$, $D_V = 0.5$) between two species increase, Rosenzweig-MacArthur model observes lattice formation under integer diffusion

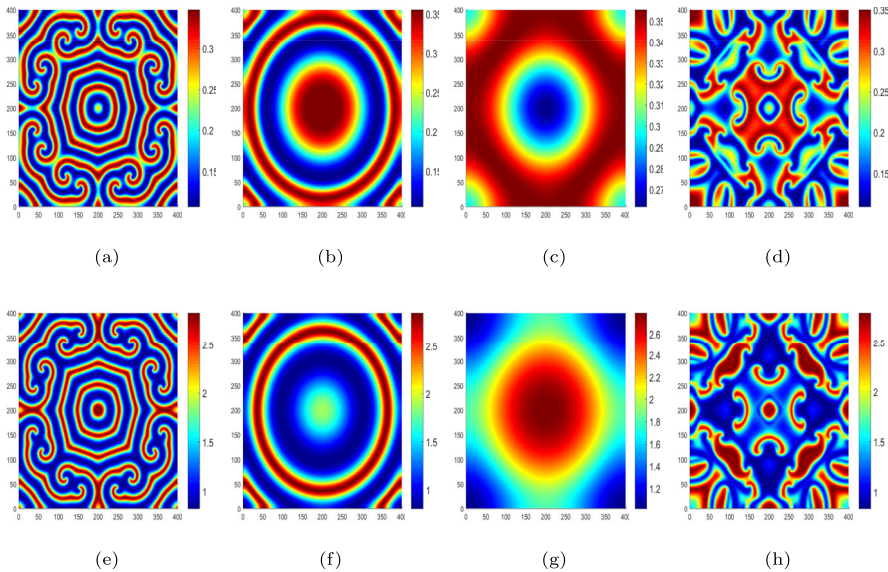


Fig. 3 Switching between symmetrical spiral patterns and concentric waves in model (2) under fractional order control: (a) $\alpha = 2$, (b) $\alpha = 1.9$, (c) $\alpha = 1.7$, and (d) $\alpha = 1.5$ for prey species or (e) $\alpha = 2$, (f) $\alpha = 1.9$, (g) $\alpha = 1.7$, and (h) $\alpha = 1.5$ for predator species. The initial value is $(U_0, V_0) = (U_*, V_*) + 0.0001 \times (1, 1)$ if $(x - 200)^2 + (y - 200)^2 < 20000$, otherwise $(U_0, V_0) = (U_*, V_*)$, and other parameters are: $D_U = 0.01$, $D_V = 0.05$, $A = 0.3$, $\beta = 5$, and $\gamma = 0.5$

$\alpha = 2$ [18]. So whether this conclusion still holds under fractional diffusion becomes a question that we need to solve in this part. We set the parameter $\beta = 12$ and diffusion coefficient $D_V = 0.5$, while keeping the remaining parameters consistent with the initial values and Fig. 3. By controlling the fractional order, we observed the evolution of the lattice formation. In addition, as the diffusion rate of the predator population increases, the average population density within the region gradually stabilizes over time, rather than exhibiting the previous periodic oscillation state. The results show that regardless of the order, the lattice formation always exists, and the fractional order only brings some subtle changes in the spatial layout (see Fig. 5).

Finally, we set the habitat as a three-dimensional space (cube), for a three-dimensional region $(x, y, z) \in \Omega = (0, 100) \times (0, 100) \times (0, 100)$, we assume a spatial step of $\Delta x = \frac{100}{101}$, a temporal step of $\Delta t = 0.1$, and a total time of $T = 5000$. The selection of its parameters and initial values will be given in each group of figure captions. Surprisingly, when the parameter values are $D_U = 0.01$, $D_V = 0.05$, $A = 0.3$, $\beta = 8$, and $\gamma = 0.5$, regardless of the fractional order, spiral patterns always appear (see Fig. 6). It should be emphasized that this is different from the discovery of 3D spiral patterns in previous time-delay systems [27], which means that even if we do not introduce new influencing factors, we will still capture such complex phenomena, which is independent of whether the habitat is two-dimensional (2D) or 3D. Furthermore, when we set the value of the parameter to $D_U = 0.01$, $D_V = 1$, $A = 0.3$, $\beta = 12$, and $\gamma = 0.5$. The formation of the 3D lattice is demonstrated, and as the fractional decreases, it follows the rule: 3D lattice formation \rightarrow 3D wave pattern \rightarrow spatially

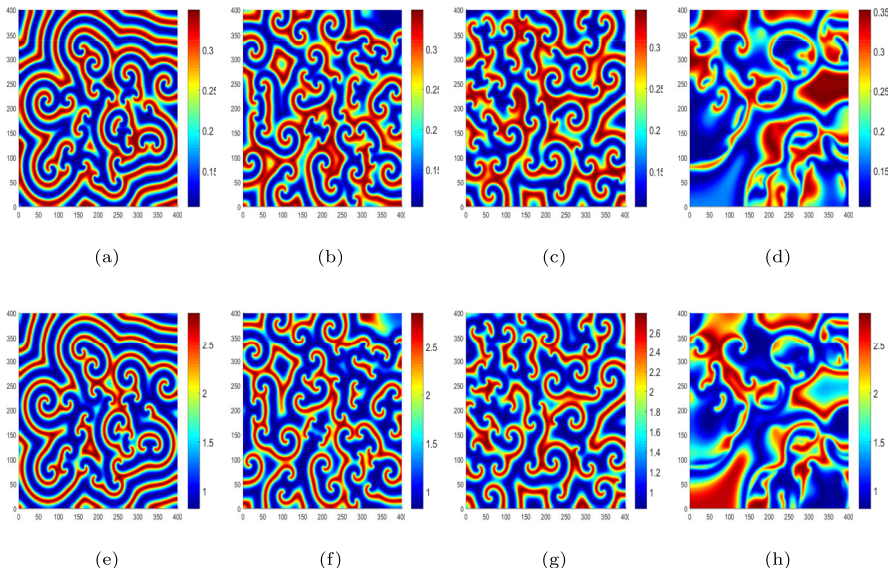


Fig. 4 Asymmetric spiral pattern in model (2) under fractional order control: **(a)** $\alpha = 2$, **(b)** $\alpha = 1.9$, **(c)** $\alpha = 1.7$, and **(d)** $\alpha = 1.5$ for prey species or **(e)** $\alpha = 2$, **(f)** $\alpha = 1.9$, **(g)** $\alpha = 1.7$, and **(h)** $\alpha = 1.5$ for predator species. The initial value is $(U_0, V_0) = (U_*, V_*) + 0.0002 \times (1, 1)$ if $(x - 300)^2 + (y - 100)^2 < 20000$ and $(x - 100)^2 + (y - 300)^2 < 10000$, $(U_0, V_0) = (U_*, V_*)$ if $(x - 300)^2 + (y - 100)^2 \geq 20000$ and $(x - 100)^2 + (y - 300)^2 \geq 10000$, otherwise $(U_0, V_0) = (U_*, V_*) + 0.0001 \times (1, 1)$, and other parameters are: $D_U = 0.01$, $D_V = 0.05$, $A = 0.3$, $\beta = 5$, and $\gamma = 0.5$

uniform distribution (see Fig. 7). To visually observe the evolution process of 3D lattice formation, we took four time points, namely $T = 500$, $T = 1500$, $T = 2500$, and $T = 3500$, and the simulation results are shown in Fig. 8.

5 Conclusions

Our work mainly explores the formation of spatial patterns in the fractional reaction-diffusion Rosenzweig-MacArthur model. The traditional view is that the spatial integer reaction-diffusion Rosenzweig-MacArthur model does not have the conditions to generate Turing patterns under classical diffusion. However, this does not mean that the model cannot produce other types of spatial patterns. In 2012, Nagano and Maeda discovered a series of beautiful and interesting spatial patterns in the spatial integer reaction-diffusion Rosenzweig-MacArthur model under appropriate initial conditions and parameters, such as spiral patterns, concentric waves, and lattice formations [18]. Considering that the diffusion form of species in large-scale spaces is likely to be Lévy diffusion, we extend this model to fractional order. We establish a fractional reaction-diffusion Rosenzweig-MacArthur model.

In theory, we have analyzed the existence and stability of equilibria within the model (2). Additionally, we have delved into thorough discussions concerning potential transcritical bifurcation, Hopf bifurcation, and stable limit cycles in the non-

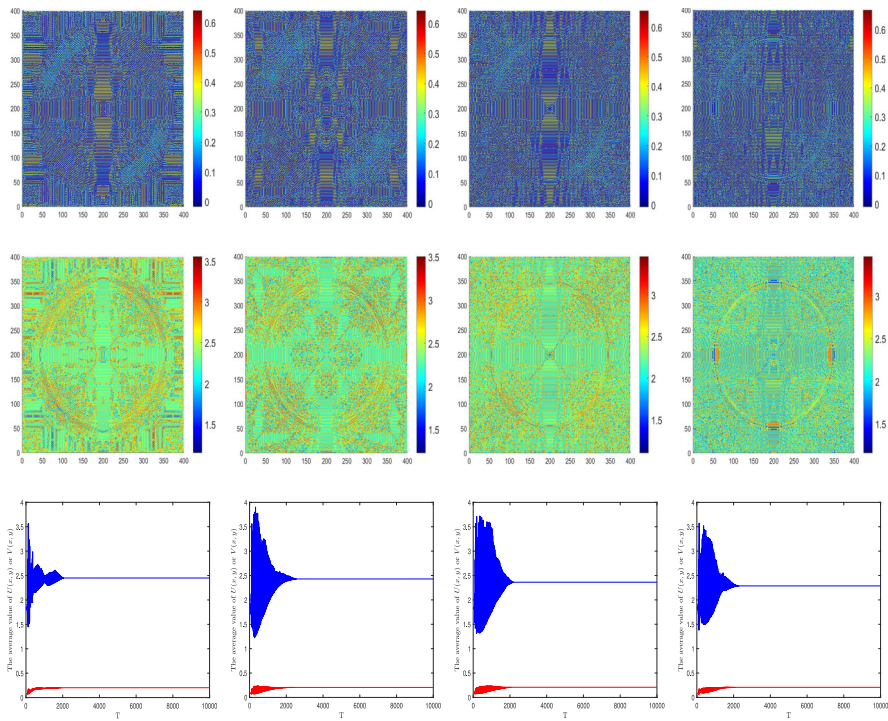


Fig. 5 The top panel represents the lattice formations of the prey population, the middle panel represents the lattice formations of the predator population, and the bottom panel depicts the evolution of average population density within this 2D region over time. From left to right, the fractional orders are $\alpha = 2$, $\alpha = 1.9$, $\alpha = 1.7$, and $\alpha = 1.5$. The initial value is $(U_0, V_0) = (U_*, V_*) + 0.0001 \times (1, 1)$ if $(x - 200)^2 + (y - 200)^2 < 20000$, otherwise $(U_0, V_0) = (U_*, V_*)$, and other parameters are: $D_U = 0.01$, $D_V = 0.2$, $A = 0.5$, $\beta = 12$, and $\gamma = 0.5$

diffusion model (2). Notably, the Hopf bifurcation observed in the spatial fractional model sets the stage for our subsequent recognition of spatiotemporal patterns. Our findings indicate that while fractional diffusion does not alter the conclusion that model (2) does not generate Turing patterns, it plays a crucial role in spatiotemporal patterns. In 2D space when appropriate initial conditions are set, both fractional and integer reaction-diffusion systems can capture spiral patterns, concentric waves, and lattice formations. The fractional order can control the switching between spiral patterns and concentric waves. Asymmetric initial conditions are easier to generate spiral patterns than symmetric initial conditions. In 3D space, we capture 3D spiral waves, 3D wave patterns, and 3D lattice formations. The decrease of fractional order also leads to the evolution of spatial patterns: 3D lattice formation \rightarrow 3D wave pattern \rightarrow spatial uniform distribution. It is worth mentioning that this may be the first time that these three types of 3D spatial patterns have been captured in a delay-free reaction-diffusion system. It can be seen that fractional order plays an important role in both 2D and 3D spaces. Therefore, fractional diffusion may be an important factor in understanding the complex spatial distribution of biological systems.

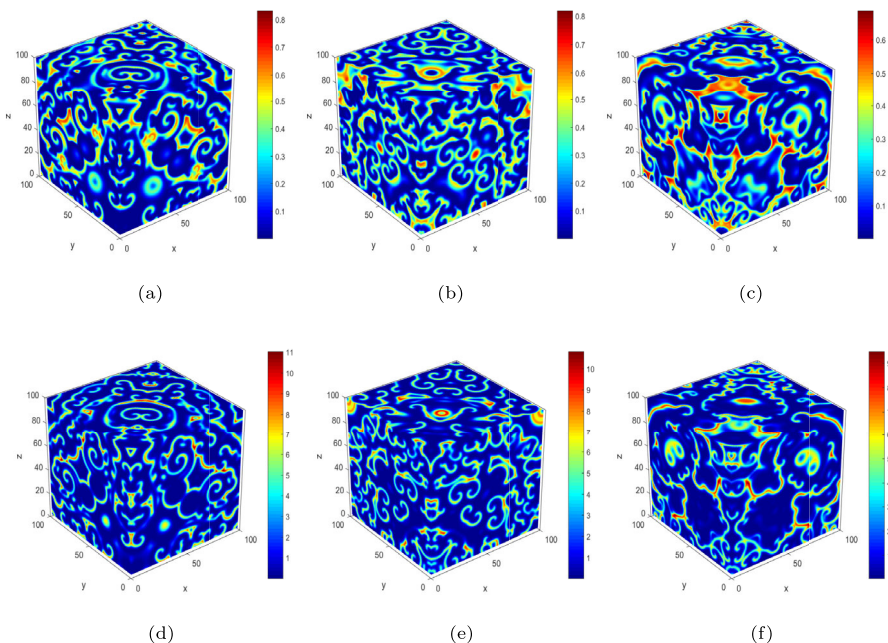


Fig. 6 3D spiral patterns in model (2) under fractional order control: **(a)** $\alpha = 2$, **(b)** $\alpha = 1.8$, and **(c)** $\alpha = 1.5$ for prey species or **(d)** $\alpha = 2$, **(e)** $\alpha = 1.8$, and **(f)** $\alpha = 1.5$ for predator species. The initial value is $(U_0, V_0) = (U_*, V_*) + 0.01 \times (1, 1)$ if $(x - 30)^2 + (y - 70)^2 < 400$, $(x - 70)^2 + (z - 30)^2 < 400$, $(z - 30)^2 + (y - 70)^2 < 400$, $(x - 70)^2 + (y - 30)^2 < 400$, $(x - 30)^2 + (z - 70)^2 < 400$, and $(z - 70)^2 + (y - 30)^2 < 400$, otherwise $(U_0, V_0) = (U_*, V_*) + 0.01 \times (1, 1)$, and other parameters are: $D_U = 0.01$, $D_V = 0.05$, $A = 0.3$, $\beta = 8$, and $\gamma = 0.5$

Rosenzweig-MacArthur model has delved deeply into the evolution of spatial patterns with fractional diffusion, yet several avenues remain for further exploration. The model primarily focuses on the spatial distribution and pattern formation of biological populations, overlooking the impact of population dynamics. Future research could integrate additional ecological factors (e.g., competition, predation, disease) to more accurately simulate the evolution of these populations. Second, while fractional diffusion shows potential in managing pattern transitions, its specific mechanisms and scope require clarification. Additionally, the model predominantly considers static or quasi-static environments, disregarding the dynamic changes that affect biologi-

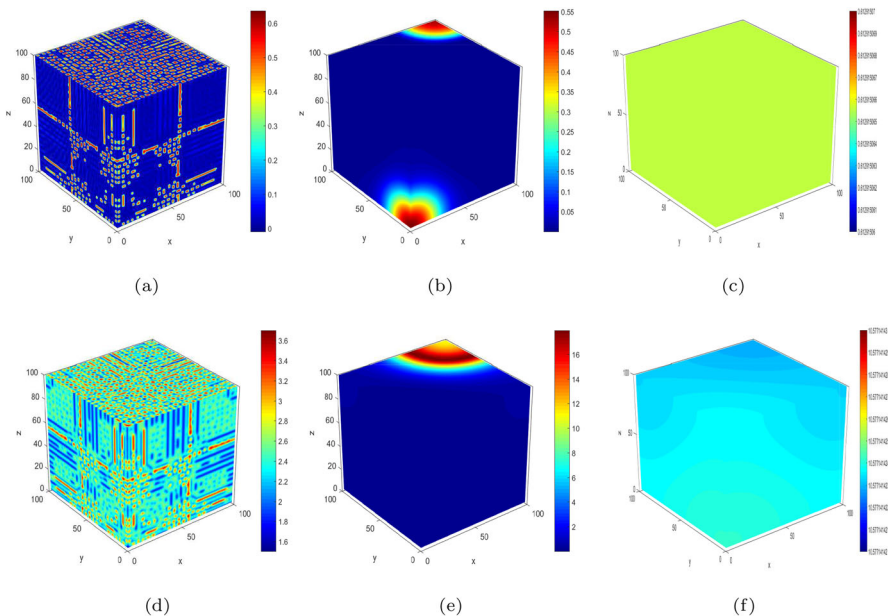


Fig. 7 The evolution of 3D patterns in model (2) under fractional order control: **(a)** $\alpha = 2$, **(b)** $\alpha = 1.8$, and **(c)** $\alpha = 1.5$ for prey species or **(d)** $\alpha = 2$, **(e)** $\alpha = 1.8$, and **(f)** $\alpha = 1.5$ for predator species. The initial value is $(U_0, V_0) = (U_*, V_*) + 0.01 \times (1, 1)$ if $(x - 30)^2 + (y - 70)^2 < 400$, $(x - 70)^2 + (z - 30)^2 < 400$, $(z - 30)^2 + (y - 70)^2 < 400$, $(x - 70)^2 + (y - 30)^2 < 400$, $(x - 30)^2 + (z - 70)^2 < 400$, and $(z - 70)^2 + (y - 30)^2 < 400$, otherwise $(U_0, V_0) = (U_*, V_*) + 0.01 \times (1, 1)$, and other parameters are: $D_U = 0.01$, $D_V = 1$, $A = 0.3$, $\beta = 12$, and $\gamma = 0.5$

cal populations (e.g., climate change, habitat modification). Future research should investigate how the model performs in these dynamic settings and how it can adapt by adjusting parameters or introducing adaptive mechanisms. In summary, Rosenzweig-MacArthur model offers a novel perspective and tool for studying spatial patterns with fractional diffusion. While it does not generate Turing patterns independently, it underscores the significance of fractional diffusion in pattern evolution. Future work should further explore this model's applications and potential to enhance our understanding of spatial pattern formation and evolution.

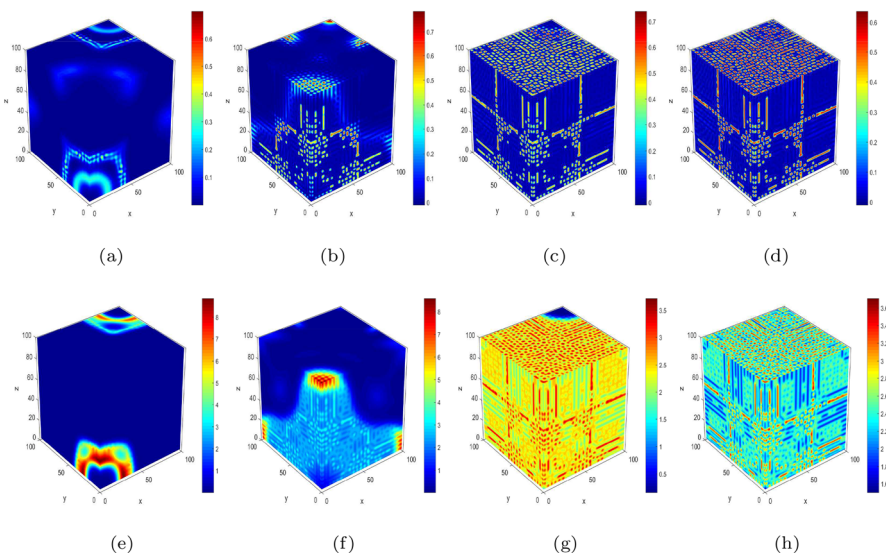


Fig. 8 Evolution of lattice formation over time in model (2): (a) $T = 500$, (b) $T = 1500$, (c) $T = 2500$, and (d) $T = 3500$ for prey species or (e) $T = 500$, (f) $T = 1500$, (g) $T = 2500$, and (h) $T = 3500$ for predator species. The initial value is $(U_0, V_0) = (U_*, V_*) + 0.01 \times (1, 1)$ if $(x - 30)^2 + (y - 70)^2 < 400$, $(x - 70)^2 + (z - 30)^2 < 400$, $(z - 30)^2 + (y - 70)^2 < 400$, $(x - 70)^2 + (y - 30)^2 < 400$, $(x - 30)^2 + (z - 70)^2 < 400$, and $(z - 70)^2 + (y - 30)^2 < 400$, otherwise $(U_0, V_0) = (U_*, V_*) + 0.01 \times (1, 1)$, and other parameters are: $D_U = 0.01$, $D_V = 1$, $A = 0.3$, $\beta = 12$, $\alpha = 2$, and $\gamma = 0.5$

Acknowledgements This work is supported by the Startup Foundation for Introducing Talent of Nanjing Forestry University (Grant No. 163101829).

Declarations

Conflict of interest The authors declare that they have no Conflict of interest.

References

1. Murray, J.D.: Mathematical Biology. Springer, Berlin (1993). <https://doi.org/10.1007/978-3-662-08542-4>
2. Xiao, D., Ruan, S.: Global analysis in a predator-prey system with nonmonotonic functional response. SIAM J. Appl. Math. **61**(4), 1445–1472 (2001). <https://doi.org/10.1137/S003613999361896>
3. Xiao, D., Ruan, S.: Global dynamics of a ratio-dependent predator-prey system. J. Math. Biol. **43**, 268–290 (2001). <https://doi.org/10.1007/s002850100097>
4. Xiang, C., Lu, M., Huang, J.: Degenerate bogdanov-takens bifurcation of codimension 4 in holling-tanner model with harvesting. J. Differential Equations **314**, 370–417 (2022). <https://doi.org/10.1016/j.jde.2022.01.016>
5. Xiang, C., Huang, J., Wang, H.: Bifurcations in holling-tanner model with generalist predator and prey refuge. J. Differential Equations **343**, 495–529 (2023). <https://doi.org/10.1016/j.jde.2022.10.018>
6. Ryu, K., Ko, W., Haque, M.: Bifurcation analysis in a predator-prey system with a functional response increasing in both predator and prey densities. In: Nonlinear Dynamics, pp. 1639–1656. (2018). <https://doi.org/10.1007/s11071-018-4446-0>

7. He, L., Zhu, L., Zhang, Z.: Turing instability induced by complex networks in a reaction-diffusion information propagation model. *Inf. Sci.* **578**, 762–794 (2021). <https://doi.org/10.1016/j.ins.2021.08.037>
8. Shi, L., Zhou, J., Ye, Y.: Pattern formation in a predator-prey model with allee effect and hyperbolic mortality on multiplex networks. *Mathematics* **11**(15), 3339 (2023). <https://doi.org/10.3390/math11153339>
9. Shi, L., Zhou, J., Ye, Y.: Global stability and hopf bifurcation of networked respiratory disease model with delay. *Appl. Math. Lett.* **151**, 109000 (2024). <https://doi.org/10.1016/j.aml.2024.109000>
10. Turing, A.: The chemical basis of morphogenesis. *Philos. Trans. R. Soc. B* **237**(641), 37–72 (1952). <https://doi.org/10.1088/rstb.1952.0012>
11. Yuan, S., Xu, C., Zhang, T.: Spatial dynamics in a predator-prey model with herd behavior. *Chaos: An Interdisciplinary Journal of Nonlinear Science* **23**(3) (2013) <https://doi.org/10.1063/1.4812724>
12. Sen, S., Ghosh, P., Riaz, S.S., Ray, D.S.: Time-delay-induced instabilities in reaction-diffusion systems. *Phys. Rev. E* **80**(4), 046212 (2009). <https://doi.org/10.1103/PhysRevE.80.046212>
13. Zhang, T., Zang, H.: Delay-induced turing instability in reaction-diffusion equations. *Phys. Rev. E* **90**(5), 052908 (2014). <https://doi.org/10.1103/PhysRevE.90.052908>
14. Liu, H., Ye, Y., Wei, Y., Ma, W., Ma, M., Zhang, K.: Pattern formation in a reaction-diffusion predator-prey model with weak allee effect and delay. *Complexity* **2019**, 6282958 (2019). <https://doi.org/10.1155/2019/6282958>
15. Hu, J., Zhu, L.: Turing pattern analysis of a reaction-diffusion rumor propagation system with time delay in both network and non-network environments. *Chaos, Solitons & Fractals* **153**, 111542 (2021). <https://doi.org/10.1016/j.chaos.2021.111542>
16. Zhu, L., He, L.: Pattern dynamics analysis and parameter identification of time delay-driven rumor propagation model based on complex networks. *Nonlinear Dyn.* **110**(2), 1935–1957 (2022). <https://doi.org/10.1007/s11071-022-07717-8>
17. Alonso, D., Bartumeus, F., Catalan, J.: Mutual interference between predators can give rise to turing spatial patterns. *Ecology* **83**(1), 28–34 (2002). [https://doi.org/10.1890/0012-9658\(2002\)083\[0028:MIBPCG\]2.0.CO;2](https://doi.org/10.1890/0012-9658(2002)083[0028:MIBPCG]2.0.CO;2)
18. Nagano, S., Maeda, Y.: Phase transitions in predator-prey systems. *Phys. Rev. E* **85**(1), 011915 (2012). <https://doi.org/10.1103/PhysRevE.85.011915>
19. Sims, D.W., Southall, E.J., Humphries, N.E., Hays, G.C., Bradshaw, C.J., Pitchford, J.W., James, A., Ahmed, M.Z., Brierley, A.S., Hindell, M.A., et al.: Scaling laws of marine predator search behaviour. *Nature* **451**(7182), 1098–1102 (2008). <https://doi.org/10.1038/nature06518>
20. Golovin, A.A., Matkowsky, B.J., Volpert, V.A.: Turing pattern formation in the brusselator model with superdiffusion. *SIAM J. Appl. Math.* **69**(1), 251–272 (2008). <https://doi.org/10.1137/070703454>
21. Zhang, L., Tian, C.: Turing pattern dynamics in an activator-inhibitor system with superdiffusion. *Phys. Rev. E* **90**(6), 062915 (2014). <https://doi.org/10.1103/PhysRevE.90.062915>
22. Bendahmane, M., Ruiz-Baier, R., Tian, C.: Turing pattern dynamics and adaptive discretization for a super-diffusive lotka-volterra model. *J. Math. Biol.* **72**, 1441–1465 (2016). <https://doi.org/10.1007/s00285-015-0917-9>
23. Ehstand, N., Kuehn, C., Soresina, C.: Numerical continuation for fractional pdes: sharp teeth and bloated snakes. *Commun. Nonlinear Sci. Numer. Simul.* **98**, 105762 (2021). <https://doi.org/10.1016/j.cnsns.2021.105762>
24. Liu, B., Wu, R., Iqbal, N., Chen, L.: Turing patterns in the lengyel-epstein system with superdiffusion. *International Journal of Bifurcation and Chaos* **27**(08), 1730026 (2017). <https://doi.org/10.1142/S0218127417300269>
25. Liu, B., Wu, R., Chen, L.: Turing-hopf bifurcation analysis in a superdiffusive predator-prey model. *Chaos: An Interdisciplinary Journal of Nonlinear Science* **28**(11) (2018) <https://doi.org/10.1063/1.5055711>
26. Liu, B., Wu, R., Chen, L.: Patterns induced by super cross-diffusion in a predator-prey system with michaelis-menten type harvesting. *Math. Biosci.* **298**, 71–79 (2018). <https://doi.org/10.1016/j.mbs.2018.02.002>
27. Bi, Z., Liu, S., Ouyang, M.: Spatial dynamics of a fractional predator-prey system with time delay and allee effect. *Chaos, Solitons & Fractals* **162**, 112434 (2022). <https://doi.org/10.1016/j.chaos.2022.112434>

28. Bi, Z., Liu, S., Ouyang, M.: Three-dimensional pattern dynamics of a fractional predator-prey model with cross-diffusion and herd behavior. *Appl. Math. Comput.* **421**, 126955 (2022). <https://doi.org/10.1016/j.amc.2022.126955>
29. Bi, Z., Liu, S., Ouyang, M., Wu, X.: Pattern dynamics analysis of spatial fractional predator-prey system with fear factor and refuge. *Nonlinear Dyn.* **111**(11), 10653–10676 (2023). <https://doi.org/10.1007/s11071-023-08353-6>
30. Rosenzweig, M.L., MacArthur, R.H.: Graphical representation and stability conditions of predator-prey interactions. *Am. Nat.* **97**(895), 209–223 (1963). <https://doi.org/10.1086/282272>
31. Perko, L.: *Differential Equations and Dynamical Systems*. Springer, New York (2013). <https://doi.org/10.1007/978-1-4613-0003-8>
32. Ouyang, Q.: *Nonlinear Science and the Pattern Dynamics Introduction* (in Chinese). Peking University Press, Beijing (2010)
33. Bueno-Orovio, A., Kay, D., Burrage, K.: Fourier spectral methods for fractional-in-space reaction-diffusion equations. *BIT Numer. Math.* **54**, 937–954 (2014). <https://doi.org/10.1007/s10543-014-0484-2>

Publisher's Note Springer Nature remains neutral with regard to jurisdictional claims in published maps and institutional affiliations.

Springer Nature or its licensor (e.g. a society or other partner) holds exclusive rights to this article under a publishing agreement with the author(s) or other rightsholder(s); author self-archiving of the accepted manuscript version of this article is solely governed by the terms of such publishing agreement and applicable law.